Article

Adsorption of CTAB on Hydrophilic Silica Studied by Linear and Nonlinear Optical Spectroscopy

Eric Tyrode, Mark W. Rutland, and Colin D. Bain

J. Am. Chem. Soc., **2008**, 130 (51), 17434-17445 • DOI: 10.1021/ja805169z • Publication Date (Web): 20 November 2008

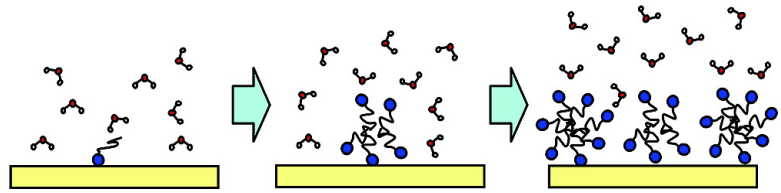

J|A|C|S
ARTICLES

Published on Web 11/20/2008

Adsorption of CTAB on Hydrophilic Silica Studied by Linear and Nonlinear Optical Spectroscopy

Eric Tyrode, Mark W. Rutland,† and Colin D. Bain*

Department of Chemistry, Durham University, South Road, Durham, DH1 3LE, United Kingdom

Received July 15, 2008; E-mail: c.d.bain@durham.ac.uk

Abstract: Vibrational sum-frequency spectroscopy (SFS) and total internal reflection Raman scattering (TIR Raman) have been used to study the adsorption of hexadecyltrimethylammonium bromide (CTAB) to hydrophilic silica. These two complementary techniques permit the determination of the adsorbed amount with a sensitivity of ~1% of the maximum surface coverage, changes in the average tilt of the adsorbed molecules, the presence of asymmetric aggregates in the adsorbed film, and the structure and orientation of the water molecules in the interfacial region. The TIR Raman spectra show a monotonic increase with CTAB concentration with no measurable changes in the relative intensities of the different polarization combinations probed, implying that no significant changes occur in the conformational order of the hydrocarbon chain. In the sum-frequency (SF) spectra, no detectable peaks from the surfactant headgroup and hydrophobic chain were observed at any surface coverage. Major changes are observed in the water bands of the SF spectra, as the originally negatively charged silica surface becomes positively charged with an increase in the adsorbed amount, inducing a change in the polar orientation of the water molecules near the surface. The detection limits for hydrocarbons chains in the SF spectra were estimated by comparison with the SF spectrum of a disordered octadecyltrichlorosilane monolayer. The simulations demonstrate that the asymmetry in the adsorbed CTAB layer at any concentration is less than 5% of a monolayer. The results obtained pose severe constraints on the possible structural models, in particular at concentrations below the critical micellar concentration where information is scarce. The formation of hemimicelles, monolayers and other asymmetric aggregates is ruled out, with centrosymmetric aggregates forming from early on in the adsorption process.

1. Introduction

The adsorption of surfactants onto hydrophilic surfaces from aqueous solutions has been studied intensively for more than half a century. A number of different models for surfactant adsorption have been proposed over the years, relating to different combinations of surfactant and surface. These models are not mutually exclusive but describe systems that lie on a continuum of possibilities between two limiting cases. One limit corresponds to surfactant molecules in which the headgroups interact only weakly with the surface. The standard free energy of binding is insufficient to compensate for the loss of translational entropy upon adsorption and the surface coverage remains negligible until the concentration is very near the critical micelle concentration (cmc). At a certain concentration, labeled the critical surface aggregation concentration (csac), aggregates adsorb to the surface. These aggregates—termed admicelles—bear a resemblance to micelles formed in the bulk phase at higher concentrations. The isotherm rises very steeply before leveling out around the cmc. At no point in the isotherm does a monolayer of surfactant form at the surface (Figure 1, sequence 1d→3d). Surfactants typically adsorb to hydrophobic surfaces at concentrations 2 orders of magnitude below the cmc.[1−4] Consequently, if a monolayer of the surfactant were to form, the hydrophobic surface thus exposed would immediately attract a second layer of adsorbed surfactant, with the opposite orientation, to eliminate the unfavorable hydrophobic interactions at the interface. This limit can be illustrated by the adsorption onto silica of nonionic surfactants, such as the polyethyleneglycol alkyl ethers with short ethylene oxide (EO) groups.[5]

The second limiting case is that of a self-assembled monolayer (the SAM limit). In a SAM, the interaction between the headgroup and the surface, augmented by van der Waals interactions between closely packed chains, is strong enough to drive monolayer formation at concentrations orders of magnitude below the cmc. A second layer does not form at these dilute concentrations because elimination of water−hydrocarbon contacts does not compensate for the loss of translational entropy upon adsorption. As the surfactant concentration is increased further, first isolated molecules adsorb to the hydrophobic surface of the SAM with the surface coverage gradually rising

† Dept. of Chemistry, Surface Chemistry, Royal Institute of Technology, Drottning Kristinas Väg 51, SE-100 44 Stockholm, Sweden and YKI, Institute for Surface Chemistry, Stockholm, Sweden.

(1) Bain, C. D.; Davies, P. B.; Ward, R. N. *Langmuir* **1994**, *10* (7), 2060–3.
(2) Fragneto, G.; Li, Z. X.; Thomas, R. K.; Rennie, A. R.; Penfold, J. *J. Colloid Interface Sci.* **1996**, *178* (2), 531–7.
(3) Fragneto, G.; Lu, J. R.; McDermott, D. C.; Thomas, R. K.; Rennie, A. R.; Gallagher, P. D.; Satija, S. K. *Langmuir* **1996**, *12* (2), 477–86.
(4) Curwen, T. D.; Bain, C. D.; Eve, J. K. *J. Phys. Chem. C* **2007**, *111* (33), 12305–12314.
(5) Bohmer, M. R.; Koopal, L. K.; Janssen, R.; Lee, E. M.; Thomas, R. K.; Rennie, A. R. *Langmuir* **1992**, *8* (9), 2228–2239.

10.1021/ja805169z CCC: $40.75

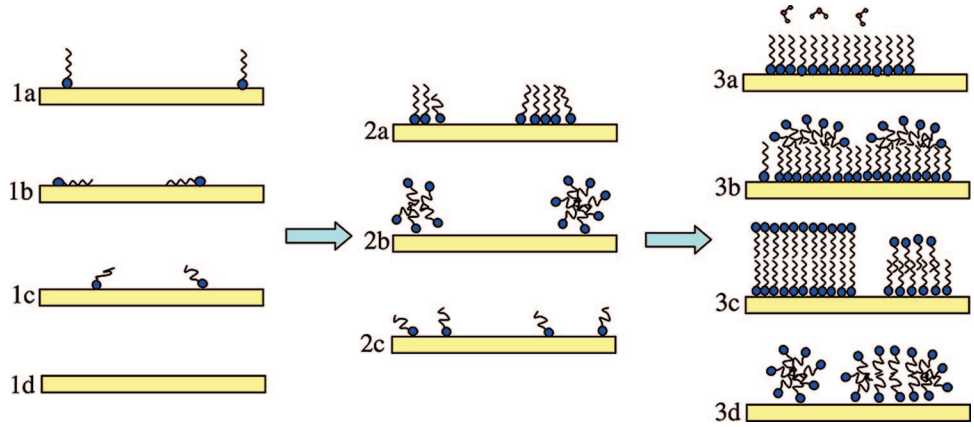

Figure 1. Cartoons displaying different morphologies that may form during the adsorption of a soluble surfactant to a clean hydrophilic substrate (1d). At very low coverages, the hydrocarbon chains of the adsorbed surfactant may be lie perpendicular to the surface (1a), parallel to the surface (1b), or be randomly oriented (1c). As the coverage increases, the molecules may be randomly distributed in a single layer (Langmuir behavior, 2c) or interactions between surfactant molecules may lead to the formation of hemimicelles (2a) or admicelles (2b). At high coverages, a range of structures are conceivable: monolayer (3a), hemimicelles on a monolayer (3b), bilayer (3c) or admicelles (3d).

until it approaches a bilayer at the cmc. This bilayer may be asymmetric, given the different nature of the interactions in the two layers (Figure 1: 1a, 1b or 1c → 2a → 3a → 3b or 3c) An example of the SAM limit is the adsorption of fatty acids on calcium fluoride.[6−8]

Other surfactant/substrate combinations lie between these two extremes with the adsorption isotherm depending on the relative adsorption energies of the surfactants to the hydrophilic surface and to a hydrophobic surface, and on the strength of interactions between chains. In the celebrated "four region model" of Somasundaran and Fuerstenau,[9] molecules first adsorb to isolated sites on the surface. As the concentration increases, chain−chain interactions lead to the formation of surface clusters, termed hemimicelles, at concentrations below those at which the surfactant adsorbs to a hydrophobic surface. In contrast to the admicelles formed with nonionic surfactants, hemimicelles are noncentrosymmetric and expose a hydrophobic surface to the aqueous solution. At higher concentrations still, a second layer of surfactant with opposite orientation condenses on top of the hemimicelles. Lateral growth of these aggregates leads to a bilayer or closely packed admicellar structure at the cmc. In an alternative model, proposed by Gao et al.,[10] adsorption to a hydrophobic surface occurs at concentrations below that of hemimicelle formation. The adsorption isotherm proceeds directly from a sparse monolayer to an admicellar structure.

In this paper we address the long-standing question of the adsorption of cationic surfactants on silica. On the basis of early studies by depletion measurements, microscopic models of the adsorbed states at different points in the isotherm were developed and subsequently revised and elaborated as new techniques such as fluorescence quenching, reflectometry and atomic force microscopy provided a wealth of new detail. The extensive literature was critically reviewed by Atkin et al. in 2003 and will not be covered in detail here.[11] The general consensus is that adsorption is initially driven by electrostatic attraction between the cationic surfactant and SiO^- groups on the surface, up to the isoelectric point of the interface. The adsorbed molecules are in a single layer and may or may not assemble into hemimicelles, depending on factors such as surface charge density and electrolyte concentration. At a higher surfactant concentration (the csac) hydrophobic interactions lead to the adsorption of additional surfactant molecules oriented preferentially with their head groups away from the surface. The adsorbed surfactant may form uniform bilayers but more commonly forms admicelles that resemble flattened versions of spherical or cylindrical micelles found in bulk solutions. Some important details of the adsorption process remain unclear, however.

One of the difficulties in distinguishing experimentally between the various possible adsorption models is that one needs to measure not only the adsorbed amount but also whether the adsorbed molecules are in the form of a bilayer or a monolayer. We resolve this difficulty by using two forms of vibrational spectroscopy, one of which (Raman scattering) is sensitive to all the adsorbed surfactant molecules and other of which (sum-frequency spectroscopy) measures only the asymmetry in the adsorbed layers.

Raman scattering has a reputation for being a weak effect: typical Raman scattering cross-sections are 10 orders of magnitude lower than infrared absorption cross-sections.[12] With the use of evanescent waves to enhance the surface signal and discriminate against bulk signals, total internal reflection Raman scattering (TIR-Raman) is in reality the most sensitive form of vibrational spectroscopy for studying adsorption on dielectric materials.[13] In our TIR-Raman experiments, an evanescent wave with a penetration depth of 60−200 nm is used to probe the adsorbed surfactant film at the silica-water interface. The relative intensities of the symmetric and antisymmetric CH_2 stretching modes is a well-established, if qualitative, measure of confor-

(6) Jang, W.-H.; Drelich, J.; Miller, J. D. *Langmuir* **1995**, *11* (9), 3491–9.
(7) Schroedle, S.; Richmond, G. L. *J. Am. Chem. Soc.* **2008**, *130* (15), 5072–5085.
(8) Becraft, K. A.; Richmond, G. L. *J. Phys. Chem. B* **2005**, *109* (11), 5108–5117.
(9) Somasundaran, P.; Fuerstenau, D. W. *J. Phys. Chem.* **1966**, *70* (1), 90–96.
(10) Gao, Y.; Du, J.; Gu, T. *J. Chem. Soc., Faraday Trans. 1* **1987**, *83* (8), 2671–2679.
(11) Atkin, R.; Craig, V. S. J.; Wanless, E. J.; Biggs, S. *Adv. Colloid Interface Sci.* **2003**, *103* (3), 219–304.
(12) Long, D. A. *Raman Spectroscopy*; McGraw-Hill: New York, 1977; p 276.
(13) Greene, P. A.; Bain, C. D. *Spectrosc. Eur.* **2004**, *16* (4), 8–15.

mational order in surfactant chains.[14] The relative intensities of the CH_2 stretching modes in s and p-polarized spectra are determined by the angle of the hydrocarbon chains: an increase in the tilt of the chains away from the surface normal increases the intensity of p-polarized spectra and decreases the intensity of s-polarized spectra.[15] Shifts in vibrational frequencies and changes in the relative intensities of vibrational modes provide additional information on the structural changes in the adsorbed film. A recent study of the main phase transition in supported phospholipid bilayers illustrates the exquisite sensitivity of TIR-Raman to both conformational order and chain tilt.[15] As a linear optical technique, TIR-Raman senses all the molecules in the adsorbed film. Bulk surfactant within the evanescent wave also contributes to the TIR-Raman spectrum, but this contribution is negligible below the critical micelle concentration of CTAB (0.92 mM).

Infrared-visible sum-frequency spectroscopy (SFS) is a second-order nonlinear optical technique and consequently only detects molecules in noncentrosymmetric environments.[16−19] Surfactants in bulk solution give no sum-frequency (SF) spectra and SFS is only sensitive to the net asymmetry in the adsorbed layer.[16] This cancelation of SF signals from molecules with opposite orientations has also been used to powerful effect in the study of supported lipid bilayers.[20,21] Frequently, SFS is employed to infer the tilt of hydrocarbon chains (from the relative intensity of the symmetric or asymmetric methyl stretches in SF spectra with different polarizations[22]) and the conformational disorder (from the ratio of line strengths of the symmetric methylene and methyl stretches[22]). Since SFS is only sensitive to the asymmetry in the adsorbed layer, it provides little useful information about the average tilt or conformation of the surfactant molecules except in systems where one knows from other experiments that all the molecules have the same polar orientation (i.e., the tilts of the molecules are either all $<90°$ or all $>90°$, depending on how the tilt angle is defined). This assumption is not valid *a priori* for adsorption of surfactants on hydrophilic surfaces, though it holds quite well in the SAM limit at low concentrations.

SFS additionally provides information on the structure of interfacial water.[18] The charge on the surface orients the first few monolayers of water, so the overall strength of the SF signal in O−H stretching region can be used to locate the isoelectric point of the surface. The sign of the surface charge can, in principle, be determined from the phase of the SF signal, but in the case of CTAB adsorption on silica it is well-known that the surface charge switches from negative to positive as the surfactant coverage increases.[23] An important feature of the O−H stretching region is the presence a free O−H stretch around 3680 cm^{-1} from water molecules in contact with a hydrophobic surface.[24] Some adsorption models generate water-hydrocarbon contacts, especially at low surface coverages, which should have a characteristic signature in the SF spectrum.

The complementarity of TIR-Raman and SFS is therefore clear: Raman yields the total coverage and average tilt; SFS yields the asymmetry in the adsorbed film relative to the plane of the surface and the sign of the surface charge. The intensity of the Raman signal is linearly proportional to the number of molecules per unit area and has sufficient sensitivity in the C−H stretching region to detect 0.05 μmol m^{-2} of CTA^+ ions, or $\sim$1% of the maximum surface coverage, as we show below. The dependence of the SF signal on surface coverage is complex because it depends, *inter alia*, on the mean orientation of the surfactant, the degree of cancelation of molecules with opposing orientations and the coherent interference with other signals, notably that from interfacial water. As a general statement, however, the quadratic dependence on the surface excess of second-order nonlinear optical processes reduces the sensitivity of SFG at low surface coverages compared to Raman scattering. The detection limit for CTAB on silica will be discussed in detail later.

2. Experimental Section

2.1. Materials. Hexadecyltrimethylammonium bromide (CTAB) and octadecyltrichlorosilane (OTS) were obtained from Aldrich. Palmitoyl-oleyl-sn-phosphatidyl-choline (POPC) was purchased from Avanti Polar Lipids. The CTAB was recrystallized three times from a 3:1 mixture of acetone/ methanol. The water used in the experiments was obtained from Millipore filtration units (18.2 MΩ cm resistivity, TOC < 4 ppb). The IR-grade fused silica hemispheres were custom- made by ISP Optics.

2.2. Total Internal Reflection (TIR) Raman Spectrometer. The Durham TIR Raman spectrometer is based on a commercial Raman microscope (Ramascope 1000, Renishaw) equipped with a 50× ULWD, 0.55 NA objective (Olympus). The pumping laser was a 532 nm *cw* frequency-doubled diode-pumped YVO_4 laser (Spectra Physics Millennia 2) which was externally delivered to the sample stage (Figure 2). The nominal power at the laser head was kept constant at 600 mW, corresponding to approximately 400 mW at the sample, with an ellipsoidal laser spot with typical size of 30 × 10 μm. Spectra are displayed in counts per second, where one count corresponds to 5 detected photons. The angle of incidence, θ, of the incident laser at the silica-water interface was 73.0° from the surface normal (critical angle = 65.8° at 532 nm), giving a penetration depth (d) for the squared evanescent field of $\sim$100 nm (eq 1)[25]

$$d = \frac{\lambda_0}{4\pi}\left(\frac{1}{\sqrt{n_{\text{silica}}^2 \sin^2\theta - n_{\text{solution}}^2}}\right) \quad (1)$$

where λ_0 is the laser wavelength in vacuum and n_j is the refractive index of medium j. The measuring cell consisted of a IR grade fused silica hemisphere (5 mm in radius) sealed with a Viton O-ring to the top of a custom-made jacketed glass cell. The silica hemisphere minimizes aberrations to the incident laser beams and collects the scattered light in a cone of angles matched to the objective's numerical aperture. The surfactant solution was injected through a glass capillary positioned a few millimeters below the center of the hemisphere, yielding stagnation point flow at the capillary position. The acquisition time for each Raman spectrum was 5−10 min, though it is possible to collect spectra with a signal-to-noise ratio of 10:1 in just a few seconds. Newly injected solutions

(14) Gaber, B. P.; Peticolas, W. L. *Biochim. Biophys. Acta, Biomembranes* **1977**, *465* (2), 260–274.
(15) Lee, C.; Bain, C. D. *Biochim. Biophys. Acta, Biomembranes* **2005**, *1711* (1), 59–71.
(16) Bain, C. D. *J. Chem. Soc., Faraday Trans.* **1995**, *91* (9), 1281–1296.
(17) Shen, Y. R. *Proc. Int. School Phys. Enrico Fermi* **1994**, *120*, 139–165.
(18) Shen, Y. R.; Ostroverkhov, V. *Chem. Rev.* **2006**, *106* (4), 1140–1154.
(19) Richmond, G. L. *Chem. Rev.* **2002**, *102*, 2693–2724.
(20) Liu, J.; Conboy, J. C. *J. Am. Chem. Soc.* **2004**, *126* (29), 8894–8895.
(21) Liu, J.; Conboy, J. C. *J. Phys. Chem. C* **2007**, *111* (25), 8988–8999.
(22) Bell, G. R.; Bain, C. D.; Ward, R. N. *J. Chem. Soc., Faraday Trans.* **1996**, *92* (4), 515–523.
(23) Parker, J. L.; Yaminsky, V. V.; Claesson, P. M. *J. Phys. Chem.* **1993**, *97* (29), 7706–7710.
(24) Du, Q.; Freysz, E.; Shen, Y. R. *Science* **1994**, *264* (5160), 826–828.
(25) Lipson, S. G.; Lipson, H.; Tannhauser, D. S. *Optical Physics*, 3rd ed.; University Press: Cambridge, 1995.

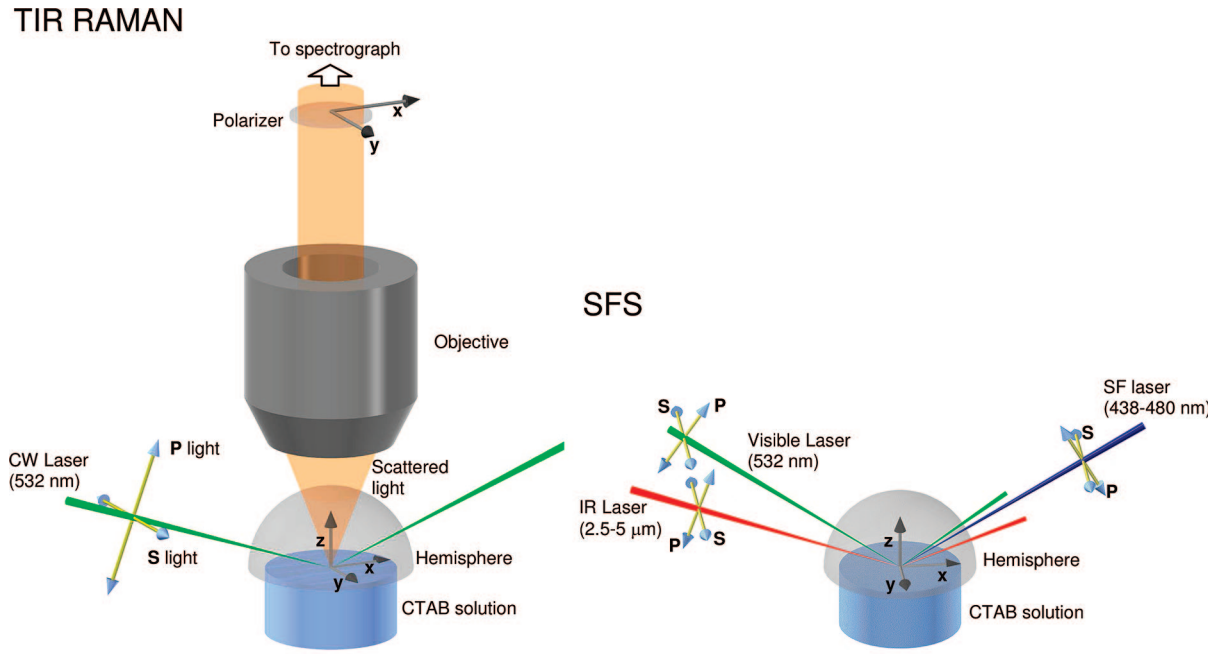

Figure 2. Diagrams of the TIR Raman and SFS setups. All laser beams propagate in the *xz* plane. In *P* polarized light the laser's electric field oscillates parallel to the plane of incidence (*xz* plane), while in *S* polarization it oscillates perpendicular to the *xz* plane.

were left to equilibrate for at least 30 min before collection of the Raman spectra under the different polarizations. All spectra were collected at 27.0 °C.

The use of different polarizations for the excitation beam (*S* or *P*), and selection of a single polarization of the scattered radiation (*x* or *y*), allows the probing of different elements of the Raman tensor, which are sensitive to the orientation of the surface molecules. Spectra collected under the *Sy* combination (incident laser "*S*" polarized and analyzer set to collect light polarized along the "*y*" axis), is most sensitive to the α'_{yy} component of the Raman tensor ($\alpha'_{xx}=\alpha'_{yy}$ for a uniaxial adsorbed layer, i.e. one that is isotropic in the plane of the surface), while *Sx* samples the off-diagonal element α'_{xy} which is equal to α'_{yx} for a uniaxial layer. *Py* and *Px* sample a combination of α'_{yz} ($=\alpha'_{xz}$ for a uniaxial layer) with α'_{yx} and α'_{xx}, respectively. The α'_{zz} element scatters light principally along the plane of the surface, which is not collected efficiently in our experimental geometry and makes a negligible contribution to the recorded *Px* and *Py* spectra.

Changes in the orientation of surface molecules can be detected in TIR Raman spectra by several means. Changes in the average tilt of an alkyl chain result in variations in the intensity of the *S* spectra (*Sx* and *Sy*) relative to the *P* spectra (*Px* and *Py*). Conformational changes, such as gauche defects, result in the variation of the relative intensity of peaks in the same spectra (e.g., the ratio of the antisymmetric to symmetric methylene stretching modes), as well as in a shift of the peak positions of certain vibrational modes.[15,26]

Bulk Contribution in the Raman Spectra. The depth of solution probed by TIR Raman is approximately 100 nm under our experimental conditions. As a consequence, contributions from surfactant molecules in the bulk may not be negligible at high concentrations. The bulk contribution increases approximately linearly with concentration and can be estimated from a linear fit to a plot of the integrated Raman intensities against concentration for solutions well above the cmc, where the amount of adsorbed surfactant is constant. This procedure may also be used to calibrate the surface coverage in TIR Raman, since the slope of the fitted line can be directly linked to the adsorbed amount provided that the penetration depth is well-known (i.e., θ is not too close to the critical angle). For ionic surfactants, some care is required since the electric double layer may lead to depletion (or enhancement below the point of zero charge) of the bulk surfactant within a few Debye lengths (κ^{-1}) of the surface. For calibration purposes, data should only be used for concentrations where the penetration depth, $d \gg \kappa^{-1}$.

2.3. Sum-Frequency Spectrometer. The Stockholm SF spectrometer has been described in detail elsewhere[27] and will be only briefly outlined here. The system consists of a Nd:YAG laser (1064 nm, 20 Hz, 24 ps) from EKSPLA, which is used to pump an OPG/OPA (LaserVision, USA), which generates the visible beam (λ = 532 nm) and the tunable infrared beam. In these particular experiments, the IR frequency ranged from 2700−4000 cm^{-1} with an average energy per pulse at the surface of 150 μJ and a bandwidth of <6 cm^{-1}. The two laser beams were transmitted through the IR grade fused silica hemisphere and overlapped in time and space at the solid/liquid interface in a copropagating geometry, with angles of incidence of 55 and 63° from the surface normal for the visible and IR beams, respectively (Figure 2). The generated SF beam was optically and spatially filtered, passed through a monochromator, and finally detected with a photomultiplier tube (PMT). The gated signal was integrated in a boxcar interfaced to a PC. The measured SF intensity was normalized by the energy of the visible and IR fields to account for power fluctuations. Experiments were performed using an identical cell to the one employed in the TIR Raman experiments. The number of scans carried out per concentration varied between 3 and 20 (180−1200 shots per point in the spectra shown), which corresponds to approximately 1 to 8 h of collection time per spectrum.

Setting the electric fields involved in the SF process to specific polarizations allows the determination of specific matrix elements of the third-rank susceptibility tensor, $\chi^{(2)}$. Symmetry constraints reduce the number of independent, nonzero tensor elements. Provided the frequencies of the lasers are far away from electronic transitions and the surface is azimuthally isotropic, out of the 27 elements, only 7 remain of which 3 are independent: $\chi_{yyz} = \chi_{xxz}$, $\chi_{yzy} = \chi_{xzx} = \chi_{zyy} = \chi_{zxx}$, and χ_{zzz}. The values of these elements can

(26) Snyder, R. G.; Hsu, S. L.; Krimm, S. *Spectrochim. Acta, Part A* **1978**, *34A* (4), 395–406.

(27) Johnson, C. M.; Tyrode, E.; Baldelli, S.; Rutland, M. W.; Leygraf, C. *J. Phys. Chem. B* **2005**, *109* (1), 321–328.

be obtained experimentally from data at different polarization combinations. For an azimuthally isotropic surface the combinations that give rise to SF signal are *SSP*, *SPS*, *PPP* and *PSS*, where the letters designate whether the beam is polarized perpendicular (*S*) or parallel (*P*) to the plane of incidence for the SF, visible, and IR beams, respectively. In this report, SF spectra were mainly collected under the *SSP* polarization combination, which specifically probes the tensor element χ_{yyz}. For *SSP* the intensity of the SF beam (I_{SF}) can be described by:[28]

$$I_{SF}(SSP) = \frac{8\pi^3\omega_{SF}^2}{c^3}\frac{\sin^2\theta_{IR}\sec^2\theta_{SF}}{n_{silica(\omega_{SF})}n_{silica(\omega_{Vis})}n_{silica(\omega_{IR})}}|L_{SF}L_{Vis}L_{IR}|^2|\chi_{yyz}|^2 I_{IR}I_{Vis} \quad (2a)$$

$$SSP\ Fresnel\ prefactors = \frac{\sin^2\theta_{IR}\sec^2\theta_{SF}}{n_{silica(\omega_{SF})}n_{silica(\omega_{Vis})}n_{silica(\omega_{IR})}}|L_{SF}L_{Vis}L_{IR}|^2 \quad (2b)$$

where n, θ, I, and L refer to the refractive index, angle of incidence, intensity, and Fresnel factors of the respective beams, and c and ω_{SF} to the speed of light in vacuum and frequency of the SF beam, respectively. The Fresnel factors relate the electric fields in the incident medium to those at the interface, and depend on the angle of the reflected (θ_i) and refracted beams (β_i), as well as the refractive indices of the interfacial layer (n') and those of the bulk media, which in our case are fused silica and the aqueous surfactant solution (which we have approximated to that of pure water):[28]

$$L_{SF} = \frac{2n_{silica(\omega_{SF})}\cos\theta_{SF}}{n_{silica(\omega_{SF})}\cos\theta_{SF} + n_{water(\omega_{SF})}\cos\beta_{SF}} \quad (3a)$$

$$L_{Vis} = \frac{2n_{silica(\omega_{Vis})}\cos\theta_{Vis}}{n_{silica(\omega_{Vis})}\cos\theta_{Vis} + n_{water(\omega_{Vis})}\cos\beta_{Vis}} \quad (3b)$$

$$L_{IR} = \frac{2n_{water(\omega_{IR})}\cos\theta_{IR}}{n_{silica(\omega_{IR})}\cos\beta_{IR} + n_{water(\omega_{IR})}\cos\theta_{IR}}\left(\frac{n_{silica(\omega_{IR})}}{n'_{(\omega_{IR})}}\right)^2 \quad (3c)$$

At the angles of incidence used in our SF experiment, the visible and SF Fresnel factors remain essentially constant over the frequency range scanned. However, the L_{IR} term varies considerably due to the strong dispersion in the refractive index of water in the IR frequency range, which goes through a maximum of $1.48 + 0.14i$ at 3150 cm^{-1} and a minimum of $1.14 + 0.11i$ at 3650 cm^{-1}.[29] Consequently the IR laser beam is totally internally reflected above ~3400 cm^{-1} where L_{IR} is seen to increase thereby enhancing the SF signal. Since we are mainly interested in the relative value of χ_{yyz}, all the SF spectra shown in this report have been normalized by the IR frequency-dependent Fresnel prefactors (eq 2b) shown graphically in Figure 3 (in the calculation of L_{IR} the refractive indices of the interfacial layer, n', were set equal to those of water at the corresponding IR frequency; a curve for n' equal to 1.4, representing a hydrocarbon environment, is shown for comparison).

Fitting of SF Spectra. The spectra were fitted by Lorentzian line shapes of the form presented in eq 4, employing the software Origin (OriginLab) and using the Levenberg−Marquardt iteration routine.

$$I_{SFG}(\omega_{IR}) = \left|A_{NR} + \sum_n \frac{A_n}{\omega_n - \omega_{IR} - i\Gamma_n}\right|^2 \quad (4)$$

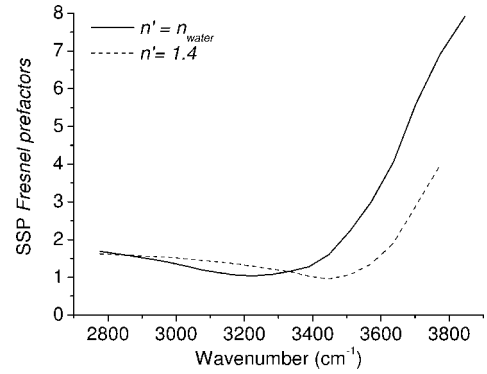

Figure 3. Fresnel prefactors for the ssp polarization combination as a function of the IR wavelength, calculated with $n' = n_{water}$ (solid line) and $n' = 1.4$ (dashed line) All the SF spectra shown in this paper were normalized by the curve with $n' = n_{water}$.

A_{NR} refers to the nonresonant contribution to the SF signal, A_n to the amplitude or oscillator strength of the nth resonant mode, and ω_{IR}, ω_n, and Γ_n, to the infrared frequency, the peak position, and damping constant of the nth resonant mode, respectively. This complex function allows for interference between overlapping bands and the nonresonant background, which is a distinctive feature of the coherent nature of the SF process. The fit could be improved by convolution of the Lorentzians with a Gaussian function to represent inhomogeneous broadening,[30] but the simpler form of eq 4 is sufficient for our purposes here.

2.4. Sample Preparation and Handling. Identical substrates, recrystallized batches of CTAB, and cleaning procedures were used in the TIR Raman and SF experiments. The IR-grade fused silica hemisphere was soaked in chromosulphuric acid for at least two hours, rinsed copiously in ultrahigh purity water, sonicated and finally rinsed once again in water. All other items including glassware, Teflon valves and tubing, and Viton O-rings, were cleaned with a commercial alkaline agent (Deconex from Borer) and rinsed thoroughly with water. Solutions were prepared in unbuffered ultrahigh purity water at ambient pH (~5.6). The CTAB concentration in the measuring cell was changed by subsequent additions of higher concentration solutions. The hydrodynamics of the cell (a wall jet) ensure rapid displacement of the previous solution. The volume added in each step was equivalent to 6 times the total cell volume to ensure that the cell is well-flushed. Once the cell was assembled the substrate remained clean for several days, as inferred from the constancy of the spectra recorded for pure water in both the TIR Raman and SF setups.

3. Results

3.1. Raman Scattering. Raman scattering is not intrinsically surface sensitive and TIR-Raman spectra therefore contain contributions from the silica substrate and the solution within the evanescent field as well as from the adsorbed surfactant layer. Figure 4A shows spectra obtained from a bare silica-water interface and from the silica-water interface in the presence of 1 mM CTAB. The strong peaks below 1300 cm^{-1} and a significant portion of the broadband at 1600 cm^{-1} are from the silica substrate while the stretching modes from water in the evanescent field are seen between 3000 and 3700 cm^{-1}. The spectrum obtained by subtracting the water reference from the surfactant spectrum is shown in Figure 4B. The C−H stretching modes of the CTAB from 2800−3000 cm^{-1}, the CH_2 scissoring mode at 1470 cm^{-1} and the CH_2 twisting/wagging mode at 1300 cm^{-1} are all clearly resolved. Lower frequency

(28) Zhuang, X.; Miranda, P. B.; Kim, D.; Shen, Y. R. *Phys. Rev. B: Condens. Matter Mater. Phys.* **1999**, *59* (19), 12632–12640.
(29) Hale, G. M.; Querry, M. R. *Appl. Opt.* **1973**, *12* (3), 555–563.
(30) Bain, C. D.; Davies, P. B.; Ong, T. H.; Ward, R. N.; Brown, M. A. *Langmuir* **1991**, *7* (8), 1563–6.

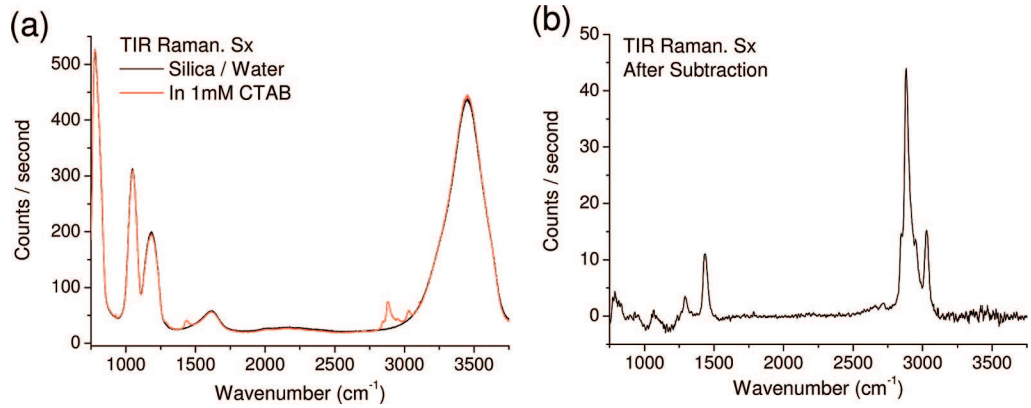

Figure 4. (a) TIR Raman spectra of silica in contact with pure water and in contact with a CTAB surfactant solution. (b) Subtracted spectra showing bands from the surfactant molecules present at the surface as well as a portion of those in the bulk probed by the evanescent field.

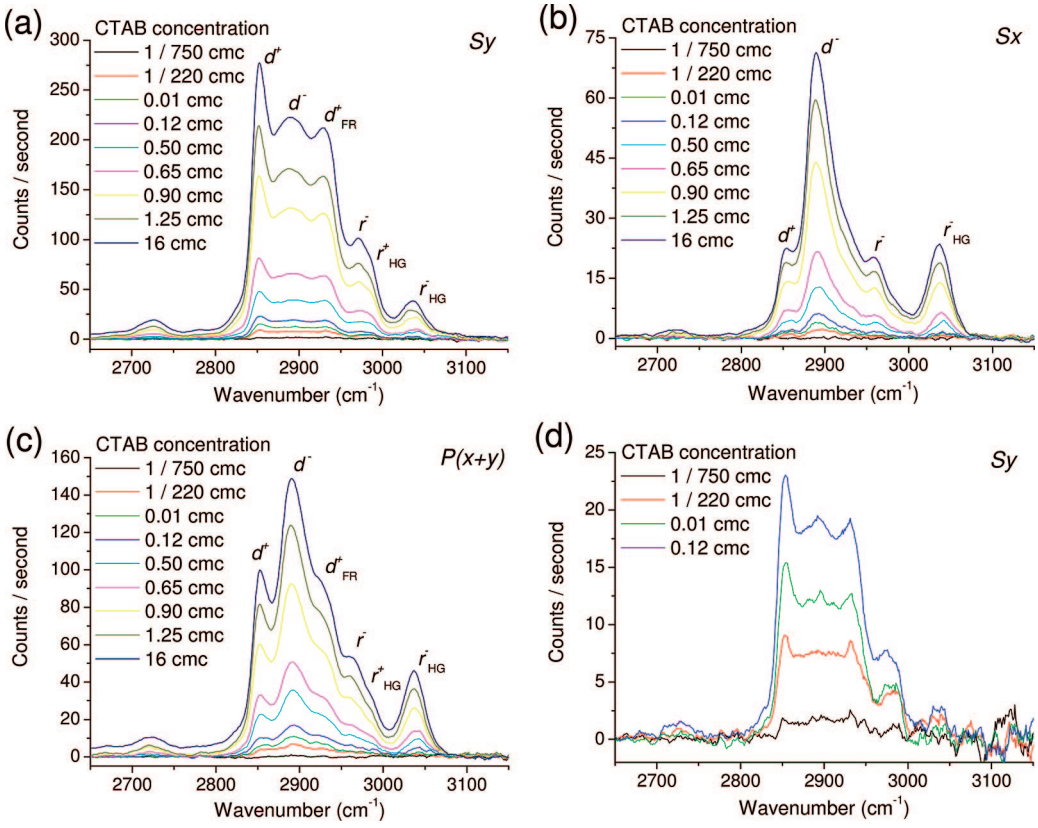

Figure 5. TIR Raman subtracted spectra of silica in contact with increasing concentration of CTAB solutions collecting under the polarization combinations (a) *Sy*, (b) *Sx*, (c) *P*(*x*+*y*), and (d) expanded plot of low concentration range in *Sy*.

modes overlap the strong substrate bands and are more difficult to resolve unambiguously. In principle, changes in water structure at the interface could be detected in O−H stretching and bending modes but slow instrumental drift masks these structural effects (which would change the OH signal strength by <1%). In the rest of this section, we will concentrate on the structurally sensitive C−H stretching modes.

TIR-Raman spectra were acquired at concentrations of CTAB ranging from 1/750 to 16 times the cmc (cmc = 0.92 mM). For each concentration three spectra were acquired with the *Sy*, *Sx*, (*Py* + *Px*) polarization combinations. Control studies showed little difference between *Px* and *Py*, so the polarizer was removed from the spectrometer to increase the signal-to-noise ratio. Figures 5A−C show a selection of these spectra for the three polarizations. The assignments of the majority of peaks observed in this spectral region are well established.[26,31] The strongest bands originate from methylene stretches, specifically the antisymmetric methylene stretch (d^+) at 2890 cm^{-1}, the symmetric methylene stretch (d^+) at 2852 cm^{-1}, and its Fermi resonance with an overtone of the CH_2 scissoring mode (d^+_{FR}) at 2928 cm^{-1}. The scattering intensity from the modes of the terminal methyl group of the alkyl chain are comparatively weaker in spite of having a larger Raman cross section,[32] due to their relatively lower number density (there is only one CH_3 per fifteen 15 CH_2 in the chain). The symmetric methyl stretch

(31) Snyder, R. G.; Strauss, H. L.; Elliger, C. A. *J. Phys. Chem.* **1982**, *86* (26), 5145–50.
(32) Colthup, N.; Daly, L. H.; Wiberley, S. E. *Introduction to Infrared and Raman Spectroscopy*, 3rd ed.; Academic Press: San Diego, 1990; p 547.

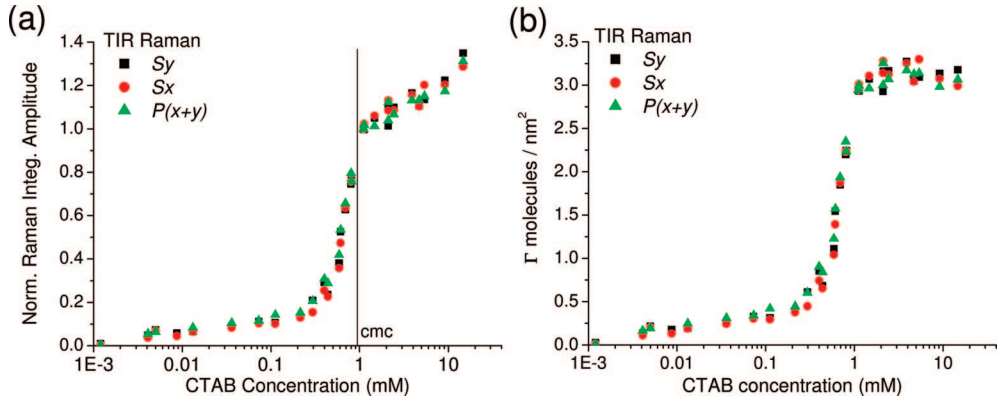

Figure 6. (a) Normalized Raman integrated intensities as a function of CTAB bulk concentration. (b) Adsorption isotherm obtained after subtraction of the bulk contribution and conversion of the Raman integrated intensities into adsorbed amounts. See text for details.

(r^+, expected at ~2870 cm^{-1}) is obscured in our spectra by the d^- mode, while the asymmetric methyl stretch (r^-) is clearly observed at ~2960 cm^{-1}. The spectral features from the methyl groups of the trimethylammonium headgroup appear at higher frequencies:[33] the symmetric stretch (r^+_{HG}) is observed as a shoulder at ~2985 cm^{-1} in the *Sy* and *P*(*x*+*y*) spectra, whereas the asymmetric stretch (r^-_{HG}) is clearly observed in all polarizations at ~3040 cm^{-1}. Finally the band detected at 2725 cm^{-1}, which is also observed in SF spectra of ordered monolayers, is tentatively assigned to an overtone of the terminal alkyl chain CH_3 deformation.

As mentioned in the Experimental Section, different elements of the Raman tensor are probed under different polarization combinations,[12] resulting in obvious differences in the spectral shapes. Symmetric vibrations, which are associated with the diagonal tensor elements, are mainly probed in the *Sy* polarization combination, while antisymmetric vibrations, linked to the off-diagonal elements, are mostly probed in the *Sx* spectra. Under the conditions of the experiment, the *P*(*x*+*y*) spectra measure a combination of both.

The peak positions and relative intensities of the different vibrational modes in Figure 5 are characteristic of hydrocarbon chains in a liquid-like environment. Nonetheless, the most striking feature is the similarity of each set of spectra, independent of concentration. In fact, if the spectra are rescaled to a common maximum intensity, the spectra in each set overlap almost perfectly. In particular, there are no changes in the intensity ratio of the symmetric (d^+) and antisymmetric (d^-) methylene stretches that would be indicative of a change in the conformational order of the hydrocarbon chain.[31,33] The peak wavenumbers of these modes are also constant to within ± 1 cm^{-1}. The only significant changes with coverage are in the antisymmetric vibrational modes of the trimethylammonium headgroup (r^-_{HG}). These modes weaken relative to the methylene modes as the concentration increases and shift to lower frequency (from 3042 to 3036 cm^{-1} at high concentrations). In the *Sx* and *P*(*x*+*y*) polarized spectra, this mode appears to be split into two components at the lowest surface coverages, with the low-frequency component growing in intensity as the surface coverage increases. This interpretation is supported by a generalized 2D correlation analysis of the *Sx* spectra (see Supporting Information).

3.2. Adsorption Isotherm. The integrated area in the C−H stretching region in each subtracted spectrum is plotted as a function of bulk concentration in Figure 6a, for all three polarization combinations. Since the raw intensities are sensitive to the choice of polarization, due both to instrumental factors and to the intrinsic differences in the spectra, the areas have been normalized to unity for the point at 1.1 mM. On this normalized basis, there is excellent agreement between the three sets of data. In particular, there are no systematic differences that might point to a change with surface coverage in the mean orientation of the hydrocarbon chains. The sensitivity of TIR Raman to small changes in the average tilt of the surfactant alkyl chain can be estimated from published spectra on phospholipids bilayers across their transition temperature,[15] where a change of 20−30° in the average tilt of the acyl chain has been inferred from X-ray diffraction data.[34] In TIR-Raman spectra, the relative intensity of the d^- mode in *S*- and *P*-polarized spectra changed by more than a factor of 2. Consequently, changes of 2−4° in the chain tilt would be easily detected.

In the absence of any changes in orientation of the adsorbed surfactant, the area under the Raman spectrum is, to a good approximation, proportional to the surface coverage. One would normally expect the adsorbed amount to remain constant above the cmc, but the experimental data show a continuing increase. At the highest concentrations, bulk surfactant within the evanescent wave makes a measurable contribution to the spectra. For example, for a 100-nm penetration depth (*d*), the amount of signal from surfactant in the evanescent wave at 10 mM is equivalent to that from a surface coverage of 1.0×10^{-6} mol m^{-2}, or about 30% of the maximum coverage. At the cmc, the bulk contribution is equivalent to that from a surface coverage of around 2% of the maximum coverage and is negligible at lower concentrations. The bulk contribution can be removed if the data are replotted on a linear scale and a straight line is fitted to the points above the cmc. In fact the bulk surfactant signal provides a useful method for calibrating the surface coverage, since the amount of surfactant sampled by the evanescent wave is known. Fitting a line to the experimental values of the normalized peak area above the cmc results in a slope of 0.02 mM^{-1}. The data in Figure 6a are replotted as a conventional adsorption isotherm in Figure 6b after removal of the bulk contribution and conversion of the Raman peak area into an adsorbed amount. The calibration procedure relies on the bulk and surface species having similar spectra and is only

(33) O'Leary, T. J.; Levin, I. W. *J. Phys. Chem.* **1984**, *88* (9), 1790–6.

(34) Seddon, J. M.; Cevc, G.; Kaye, R. D.; Marsh, D. *Biochemistry* **1984**, *23* (12), 2634–44.

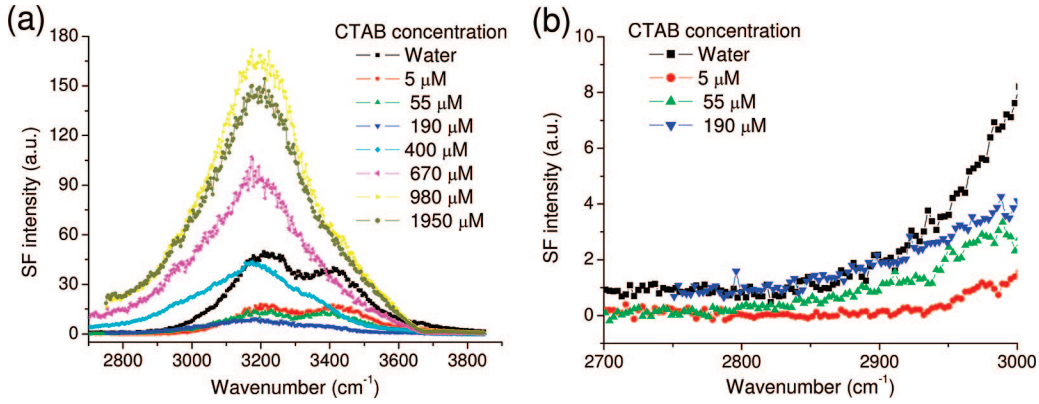

Figure 7. (a) Sum-frequency spectra of the silica/solution interface at increasing CTAB concentrations collected under the SSP polarization combination. (b) Enlarged plot of the C−H stretching region for low surfactant concentrations. Note the absence of CH stretching vibrations.

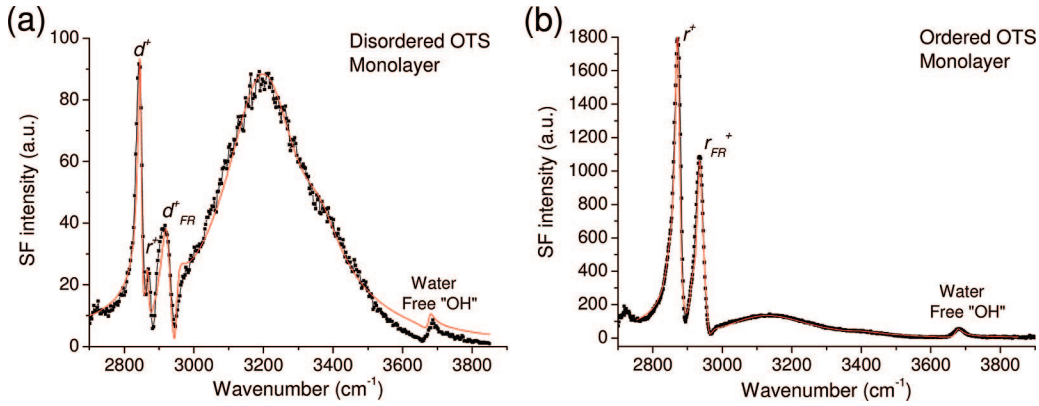

Figure 8. (a) SF spectra of a disordered octadecyltrichlorosilane (OTS) on silica in contact with water collected under the SSP polarization combination. (b) SF spectra of an ordered OTS monolayer at the silica/water interface. The scales in the two figures are comparable. The fitted curves are shown on top of each spectrum as continuous red lines.

approximate for reasons discussed in the Experimental Section, but the plateau coverage nevertheless falls within the range of values reported elsewhere (see Discussion Section).

3.3. Sum-Frequency Spectroscopy. Figure 7a shows sum-frequency spectra of the fused silica/solution interface obtained with the SSP-polarization combination for pure water and for seven selected CTAB concentrations ranging between 0.005 mM and 2 mM. Spectra were also acquired using the polarization combinations PPP and SPS but did not provide any additional insights and will not be discussed here (selected spectra collected under these two polarization combinations can be found in the Supporting Information). The spectral range recorded includes both the C−H and O−H stretches. As the surfactant concentration is raised, the overall SF signal initially decreases and then increases again. The dominant feature in the SF spectra arises from water in the electrical double layer that has been oriented by the electric field of the surface charge. As positively charged surfactant adsorbs to the negatively charged silica surface, the charge first decreases until the isoelectric point is reached then changes sign and increases again in magnitude as further cationic surfactant molecules condense onto the surface under the influence of hydrophobic interactions. The subtler features of the SF spectra of water will be discussed below, but we first address the most important feature of these spectra, namely the absence of any detectable peaks from the hydrocarbon chains of the surfactant at any surface coverage (see Figure 7b where the C−H stretching region is shown in detail). The implication of the absence of the C−H modes is that the distribution of orientations of the surfactant chains is always symmetric with respect to the surface plane. The consequence of this conclusion for models of surfactant adsorption is so profound that it is essential to establish the limits of detectability of these absent modes.

In the Introduction, we noted that the quadratic dependence of the SF signal on surface coverage places limits on the sensitivity of sum-frequency spectroscopy. Given that calculations of absolute intensities in SFS are difficult, we have estimated the detection limits for hydrocarbon chains by comparison with a SF spectrum taken under the same experimental conditions for a disordered monolayer of octadecyltrichlorosilane (OTS) on silica, which we use as a model for a typical surfactant orientation.

In Figure 8a such a spectrum for an OTS monolayer is shown. The strongest peaks in the C−H stretching region originate from methylene vibrations (the symmetric stretch d^+ at 2845 cm^{-1} and its Fermi resonance d^+_{FR} at 2920 cm^{-1}), while the terminal methyl r^+ at 2872 cm^{-1} is much weaker. In SFS, the ratio of r^+ and d^+ amplitudes, $A(r^+)/A(d^+)$ is a useful indicator of the degree of conformational order in the monolayer.[22,35] In Figure 8a, $A(r^+)/A(d^+) < 0.25$ and is indicative of a particularly disordered OTS monolayer ($A(r^+)/A(d^+)$ for a saturated CTAB monolayer at the air/water interface is close to one[36]). A densely packed OTS monolayer is shown for comparison in Figure 8b. Here the d^+ mode is almost undetectable, with $A(r^+)/A(d^+) > 60$: in

(35) Guyot-Sionnest, P.; Hunt, J. H.; Shen, Y. R. *Phys. Rev. Lett.* **1987**, *59* (14), 1597–600.
(36) Bell, G. R.; Manning-Benson, S.; Bain, C. D. *J. Phys. Chem. B* **1998**, *102* (1), 218–222.

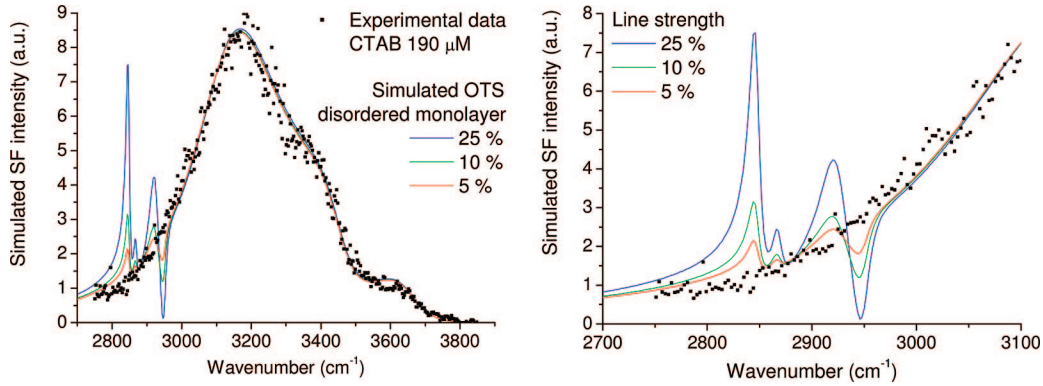

Figure 9. Simulated SF spectra of a model disordered surfactant monolayer, with varying line strengths, expressed as a fraction of a disordered OTS monolayer. The C−H stretching region is enlarged in the right-hand figure. The 190 μM CTAB spectrum was used as starting point.

an all-trans hydrocarbon chain configuration, the methylene groups are in a locally centrosymmetric environment, rendering the CH_2 vibrations virtually SF-inactive. Note also that the absolute intensities are an order of magnitude higher than in the disordered OTS spectrum of Figure 8a. The increase in signal is primarily due to a narrower distribution of angles of the alkyl chains.

We also note the "free OH" band centered at 3680 cm^{-1}, which originates from those water molecules having a non-hydrogen bonded OH group oriented toward the hydrophobic surface.[24,37,38] Its presence signifies that alkyl chains are in direct contact with water. The free OH peak is weaker in the spectrum of the disordered OTS monolayer than the ordered monolayer, but is still readily detectable.

We have fitted the SF spectrum of OTS in Figure 8a using eq 4 for 7 resonant modes (4 C−H, 3 O−H stretches; the nonresonant background was constrained to be real) and used the same fitting parameters to model the C−H peaks in our surfactant layer. In order to estimate the SF detection limits for a disordered monolayer, we simulated spectra based on the experimental spectra from CTAB solutions to which we added C−H modes with varying fractions of the line strength recorded in the disordered OTS spectrum (details of the calculation may be found in the Supporting Information). In Figure 9, we use the spectrum of 190 μM CTAB as the starting point. By comparing the simulated intensity of the C−H modes with the noise in the spectra, we determined that the detection limit is lower than 5% of a full disordered monolayer (and less than 1% for an ordered monolayer equivalent to the silane of Figure 8b). These simulations demonstrate that the asymmetry in the adsorbed CTAB layer at any concentration is less than 5% of a monolayer.

As mentioned in the Introduction, second-order nonlinear optical processes do not occur in media with an inversion center, which is in essence the property responsible for the intrinsic surface specificity of SFS. These symmetry constraints also apply to adsorbed molecules, resulting in cancelation of the sum-frequency fields from opposing groups within aggregates with a local center of symmetry. This cancelation has been reported in multilayer Langmuir−Blodgett films of fatty acid molecules, where the spectra originate exclusively from the top and/or bottom monolayers, irrespective of the number of layers present

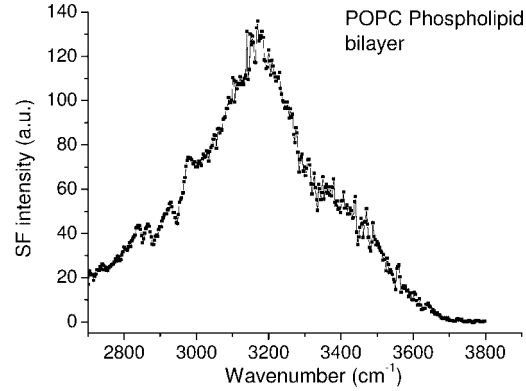

Figure 10. SF spectrum of POPC bilayer on fused silica immersed in a buffer solution (TRIS 10 mM, pH = 7.4). The spectrum was collected with SSP polarization.

in the film.[39−41] Moreover, small molecules at the liquid−air interface that form centrosymmetric species (i.e., acetic acid cyclic dimers[42]) display an analogous cancelation of the SF signal dictated by the symmetry of the molecular species. A particularly useful comparison for the CTAB films is provided by solid-supported phospholipid bilayers.[21,43] While one might expect that SF spectra from the two leaflets of the bilayer would cancel, there are subtle differences in the orientation of the chains in the two leaflets even for bilayers formed from a single phospholipid. Figure 10 shows the SF spectrum of a POPC phospholipid bilayer formed by fusion of small unilamellar vesicles onto a silica hemisphere, as described in detail elsewhere.[15] Though the spectrum is dominated by water vibrations, distinct bands can nevertheless be observed in the C−H stretching region, with the appearance of dips rather than peaks due to interference with the neighboring water bands. These features stem from slight differences in the packing of the inner and outer leaflets, which break the centrosymmetry of the bilayer. The absence of such features in the CTAB spectra in Figure 7 demonstrate that the CTAB aggregates at the silica−water interface are substantially more symmetric than a supported phospholipid bilayer in a fluid phase.

(37) Scatena, L. F.; Brown, M. G.; Richmond, G. L. *Science* **2001**, *292* (5518), 908–912.
(38) Ye, S.; Nihonyanagi, S.; Uosaki, K. *Phys. Chem. Chem. Phys.* **2001**, *3* (16), 3463–3469.
(39) Holman, J.; Davies, P. B.; Neivandt, D. J. *J. Phys. Chem. B* **2004**, *108* (4), 1396–1404.
(40) Nishida, T.; Johnson, C. M.; Holman, J.; Osawa, M.; Davies, P. B.; Ye, S. *Phys. Rev. Lett.* **2006**, *96* (7), 077402/1–077402/4.
(41) Holman, J.; Davies, P. B.; Nishida, T.; Ye, S.; Neivandt, D. J. *J. Phys. Chem. B* **2005**, *109* (40), 18723–18732.
(42) Tyrode, E.; Johnson, C. M.; Baldelli, S.; Leygraf, C.; Rutland, M. W. *J. Phys. Chem. B* **2005**, *109* (1), 329–341.
(43) Liu, J.; Conboy, J. C. *J. Am. Chem. Soc.* **2004**, *126* (27), 8376–8377.

3.4. Water Structure. We briefly comment on the features of the O−H stretching region of the spectra presented in Figure 7, noticing first that there is no evidence for a sharp "free-OH" band at ∼3680 cm^{-1} in the spectra of CTAB layers at any concentration. Two prominent broad bands centered at around 3150−3200 cm^{-1} and 3400−3450 cm^{-1} are present in all spectra, originating from water molecules with a preferred orientation in the surface region. These bands have previously been observed in the SF spectrum of fused silica and crystalline quartz in water and are loosely referred to as "ice-like" and "liquid-like" in accordance to the position of the dominant bands observed in the bulk IR and Raman spectra of ice and liquid water, respectively.[44] A third, weaker band at ∼3630 cm^{-1} (clearly observed in Figure 9 and in the enlarged spectra presented in the Supporting Information) is tentatively assigned to an Si−OH stretch from the silica substrate since this band is also present in a Raman spectrum of the silica hemisphere in dry air. Such a high frequency is characteristic of OH bonds that are freely vibrating or only very weakly hydrogen bonded.[45] The fact that the frequency of this band remains unchanged even when immersed in water suggests that the silanols responsible for this band are unavailable to water molecules. The possible presence of substrate bands in SF-spectra of silica in the OH region has not been considered previously.[46]

The variation in the absolute intensity of the two strong water bands with CTAB concentration can be attributed to variations in the surface charge. In water (pH ∼ 5.5) the fused silica surface is partially deprotonated and consequently negatively charged.[44,47] The surface field induces a preferred orientation of the dipoles of the interfacial water molecules with their hydrogen atoms facing the surface. The induced polar orientation can extend over several molecular layers and is correlated with the surface field strength.[48] With the addition of the positively charged CTAB, the surface charged is first neutralized and later becomes positively charged, as additional surfactant adsorbs to the surface. This change is reflected in the SF spectra by a fall in the signal from the water bands as the surface charge is first neutralized, followed by a subsequent increase as the interfacial water molecules reorient at the positively charged surface with their hydrogen atoms facing toward the bulk solution. Displacement of water molecules from the surface may also contribute to the initial decrease in signal. The observed surface charge reversal is corroborated by previous surface force[23,49] and streaming potential measurements[50] where the surface potential was observed to go through zero at ∼10−60 μM. The minimum in the water signal in the SF spectra occurs at higher concentrations (∼190 μM), but this difference may simply reflect different pretreatments of the silica surface.

Due to the coherent nature of the SF process, information is carried not only in the magnitude of the SF signal but also in its phase.[18] Measuring the phase during the adsorption process would unequivocally prove that the interfacial water molecules are changing their polar orientation, as the phase of the emitted light would change by π. For this purpose, a reference (internal or external) of known phase is required.[51−53] The nonresonant background from the silica substrate, though weak, serves as such a reference. When the surface is negatively charged, constructive interference with the nonresonant background results in an extended tail at high wavenumbers (Figure 7 at low surfactant concentrations); for a positively charged surface (high CTAB concentrations) there is destructive interference at high wavenumbers and constructive interference at low wavenumbers, resulting in a detectable tail in the OH signal even below 2800 cm^{-1}.

Other subtler features in the water bands warrant a brief mention. First is the apparent increase in the intensity of the "ice-like" band relative to the "liquid-like" band at the highest surfactant concentrations, as well as a shift in its peak position to lower wavenumbers. Both elements point toward interfacial water molecules becoming more "ice-like". This effect is most probably linked to an increase in the surface charge. Second is the fall in intensity observed in the water bands at concentrations above the cmc, where the surface coverage does not change significantly (Figure 7). This variation can be correlated to an increase in the ionic strength which screens the surface electric field responsible for ordering the surface water molecules (the Debye length decreases from ∼10 nm at cmc to ∼7 nm at 2 mM).

4. Discussion

Adsorption of CTAB to silica without added salt has been extensively studied in the past. The isotherm has been repeatedly measured using diverse techniques including solution depletion,[54] ellipsometry,[55] optical reflectometry,[50,56,57] and neutron reflection.[58] Although there is some scatter in the data found in the literature, the surface excess above the cmc and the overall shape of the isotherm (displaying a double plateau or "Langmuir-S shape") are comparable to those depicted in Figure 6b. Information on the lateral structure of the adsorbed layer has been obtained by atomic force microscope (AFM). The formation of distinct aggregates was first detected at concentrations just below the cmc, with peak-to-peak distances between aggregates in the order of 10 nm for concentrations above the cmc.[56,59] There is some disagreement in the literature concerning the shape of the aggregates: either spherical[59,60] (full micelle or a half-micelle on a flat monolayer) or rod-like,[56] though the coexistence of spherical and short rods was reported in the latter study at a concentration just below the cmc. Neutron reflectivity (NR) provides limited in-plane resolution but has high resolution in the direction perpendicular to the surface. NR studies have

(44) Ostroverkhov, V.; Waychunas, G. A.; Shen, Y. R. *Chem. Phys. Lett.* **2004**, *386* (1−3), 144–148.
(45) Tyrode, E.; Johnson, C. M.; Kumpulainen, A.; Rutland, M. W.; Claesson, P. M. *J. Am. Chem. Soc.* **2005**, *127* (48), 16848–16859.
(46) Zhang, L.; Tian, C.; Waychunas, G. A.; Shen, Y. R. *J. Am. Chem. Soc.* **2008**, *130* (24), 7686–7694.
(47) Ong, S.; Zhao, X.; Eisenthal, K. B. *Chem. Phys. Lett.* **1992**, *191* (3−4), 327–35.
(48) Watanabe, M.; Brodsky, A. M.; Reinhardt, W. P. *J. Phys. Chem.* **1991**, *95* (12), 4593–6.
(49) Rutland, M. W.; Parker, J. L. *Langmuir* **1994**, *10*, 1110–1121.
(50) Theodoly, O.; Cascao-Pereira, L.; Bergeron, V.; Radke, C. J. *Langmuir* **2005**, *21* (22), 10127–10139.
(51) Ostroverkhov, V.; Waychunas, G. A.; Shen, Y. R. *Phys. Rev. Lett.* **2005**, *94* (4), 046102/1–046102/4.
(52) Wei, X.; Miranda, P. B.; Zhang, C.; Shen, Y. R. *Phys. Rev. B: Condens. Matter Mater. Phys.* **2002**, *66* (8), 085401/1–085401/13.
(53) Tyrode, E.; Johnson, C. M.; Rutland, M. W.; Day, J. P. R.; Bain, C. D. *J. Phys. Chem. C* **2007**, *111* (1), 316–329.
(54) Bijsterbosch, B. H. *J. Colloid Interface Sci.* **1974**, *47* (1), 186–98.
(55) Eskilsson, K.; Yaminsky, V. V. *Langmuir* **1998**, *14* (9), 2444–2450.
(56) Velegol, S. B.; Fleming, B. D.; Biggs, S.; Wanless, E. J.; Tilton, R. D. *Langmuir* **2000**, *16* (6), 2548–2556.
(57) Atkin, R.; Craig, V. S. J.; Wanless, E. J.; Biggs, S. *J. Colloid Interface Sci.* **2003**, *266* (2), 236–244.
(58) McDermott, D. C.; McCarney, J.; Thomas, R. K.; Rennie, A. R. *J. Colloid Interface Sci.* **1994**, *162* (2), 304–10.
(59) Ducker, W. A.; Wanless, E. J. *Langmuir* **1999**, *15* (1), 160–168.
(60) Liu, J.-F.; Ducker, W. A. *J. Phys. Chem. B* **1999**, *103* (40), 8558–8567.

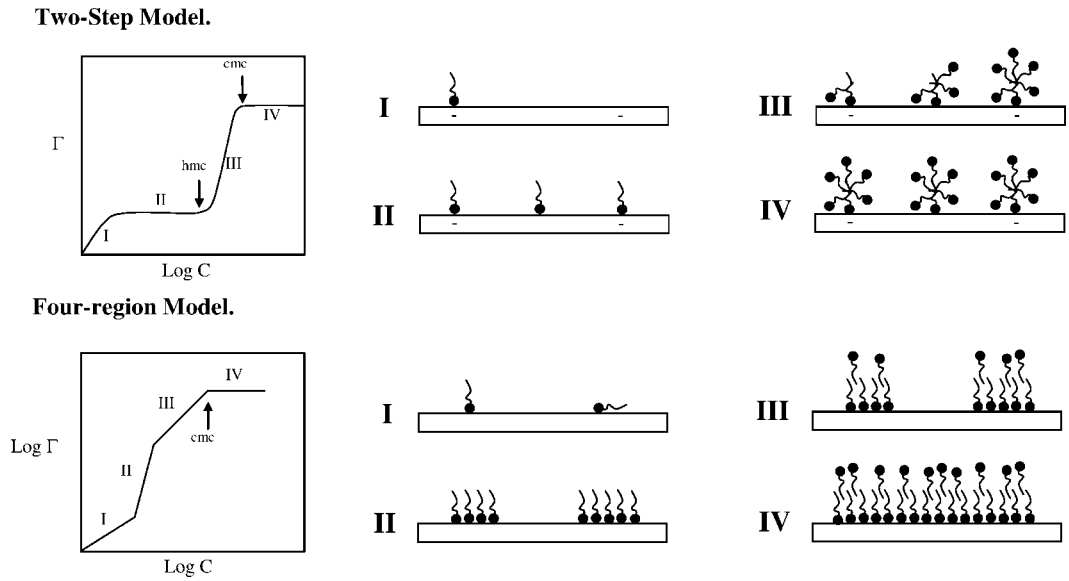

Figure 11. General shape of the adsorption isotherm and proposed molecular model for the two-step and four-region adsorption models. Adapted from refs 10 and 9, respectively.

established that the surface is always incompletely covered (consistent with the AFM results) and, importantly, that the thickness of the surfactant layer remain essentially constant in the range of 2.8−3.4 nm down to concentrations as low as 0.01 cmc.[58,61] This thickness is larger than a fully extended CTAB molecule but significantly less than twice that length.

Structural information on the adsorbed layer much below the cmc is limited: AFM does not give resolved images at low surface densities while the interpretation of the NR results is model-dependent and has provided little information beyond the overall thickness of the adsorbed layer. However, the adsorbed layer morphology in this concentration range is essential for distinguishing among different adsorption mechanisms. Two principal models have been proposed in the literature to describe the adsorption of ionic surfactants to hydrophilic surfaces: the so-called two-step model,[10,62] and the four-region model.[9,63] The general shape of the adsorption isotherm as well as the proposed molecular description of the different adsorption stages are depicted in Figure 11 for these two models. In both models, the adsorption isotherm is determined by an interplay of electrostatic and hydrophobic interactions. At the lowest concentrations (region I in both models) the surfactant adsorbs via electrostatic interactions to oppositely charged surface sites. At the highest concentrations (around the cmc), hydrophobic interactions lead to the formation of aggregates or admicelles at the solid−water interface (region IV in both models). Where the two models differ is in the relative importance of electrostatic and hydrophobic interactions at intermediate concentrations. In the two-step model there is only ever a low coverage of (isolated) molecules bound electrostatically to the substrate, which then nucleate the formation of admicelles in the steeply rising part of the isotherm. In the four-region model, there is stronger adsorption at low concentrations leading to the formation of hemimicelles before the attachment of a second layer through hydrophobic interactions. These models are not mutually exclusive; rather, they describe systems lying at different points along the continuous spectrum of possibilities between the SAM limit and the weak adsorption limit described in the Introduction. These two models provide a useful framework for discussing the Raman and SFS data presented in this paper, though neither of them accurately describes the adsorption of CTAB on silica.

The CTAB adsorption isotherm shown in Figure 6b closely resembles the double plateau curve of the two-step model of Figure 11. In the lowest surface density range (region I), specifically at concentrations below ∼4 μM when the area per surfactant molecule is larger than ∼500 Å^2, interactions between surfactant molecules are negligible and the adsorbed amount is expected to increase linearly with concentration (Henry range). TIR Raman has the sufficient sensitivity to provide information in this range. No difference in the mean orientation of the hydrocarbon chains of the surfactant was detected between low and high coverages, ruling out the possibility of finding flat-lying molecules at low surface densities. SFS is insufficiently sensitive to provide information on the polar orientation of the adsorbed CTAB molecules in the Henry range.

In the first plateau (region II); which extends from ∼4−300 μM, SFS excludes the formation of a CTAB monolayer or any other asymmetric aggregate, including hemimicelles. This provides strong evidence that hydrophobic interactions generate symmetric aggregates early on in the adsorption process. The variation in the SF water band intensities also indicates that the surface charge is neutralized at roughly 100 μM, becoming positively charged thereafter. The TIR-Raman spectra are consistent with these results: no significant changes occur in the mean orientation of the surfactant hydrocarbon chains or the trimethylammonium headgroups in this region. In fact the only variation observed, besides the monotonic increase of the Raman signal with concentration, occurs in the following concentration region (region III) where the adsorbed amount steeply rises. Here, the doublet associated with the antisymmetric methyl stretch of the headgroup (r^-_{HG}) increases asynchronously (Supporting Information). We believe the splitting results from two different environments in which the trimethylammonium group vibrates. The higher frequency component is linked to

(61) Fragneto, G.; Thomas, R. K.; Rennie, A. R.; Penfold, J. *Langmuir* **1996**, *12* (25), 6036–6043.
(62) Rupprecht, H.; Gu, T. *Colloid Polym. Sci.* **1991**, *269*, 506–522.
(63) Fan, A.; Somasundaran, P.; Turro, N. J. *Langmuir* **1997**, *13* (3), 506–510.

the headgroup interacting with specific sites of the silica substrate and its intensity is seen to stagnate in region III. On the contrary, the lower frequency component increases considerably as hydrophobic interactions drive the adsorption.

Our results place severe constraints on the possible adsorption models of CTAB to silica. In region I, surfactant molecules do not lie flat with their alkyl chains on the surface. (SFS is insufficiently sensitive in this range to provide information on the asymmetry of the adsorbed layer.) Hydrophobic interactions come into play from the beginning of region II as suggested by the four-region model, though hemimicelles do not form in this or subsequent regions (only centrosymmetric aggregates seem to form). Initial aggregates nucleate at specific sites of the silica surface, possibly where electrostatic interactions anchored the first surfactant molecules at the beginning of the adsorption process. The morphological changes along the adsorption of CTAB to silica can be illustrated by the sequence 1c→2b→3d of the sketches presented in Figure 1. One question that remains unanswered is the nature of the aggregates in region II: while SFS tells us they are centrosymmetric and Raman tells us that the orientation of the chains is the same as at high concentrations, neither technique provides information on the size of the aggregates or their distribution on the surface.

The methodology that we have demonstrated in this paper is applicable to the adsorption of any surfactant on a transparent substrate; however, the details of the mechanistic information are specific to CTAB on silica. The balance between specific surfactant/substrate interactions and hydrophobic interactions will locate any particular system somewhere on the continuum of possibilities between the SAM limit and weak adsorption limit discussed in the Introduction. If CTAB is replaced by the 12-carbon homologue, dodecyltrimethylammonium bromide, the hydrophobic interactions are relatively weaker. SF spectra then show measurable C−H peaks indicative of asymmetry in the adsorbed layer.[64] Increasing the strength of the headgroup-substrate interaction also leads to monolayers or asymmetrical aggregates, as shown in recent SFS in the adsorption of fatty acids[8] and sodium dodecyl sulfate[65] to CaF_2.

(64) Ward, R. N.; Bain, C. D. unpublished results.
(65) Becraft, K. A.; Moore, F. G.; Richmond, G. L. *J. Phys. Chem. B* **2003**, *107*, 3675–3678.

5. Conclusions

In this paper we have demonstrated the value of using SFS and TIR Raman spectroscopy in combination to study the adsorption of surfactants on hydrophilic surfaces. Both provide chemical and orientation information, but SFS has the unique ability to detect the net asymmetry in the adsorbed layer, while TIR Raman detects all the adsorbed molecules. We have used this powerful combination to revisit an old problem: the adsorption of the cationic surfactant, CTAB, on silica. We have shown that the average orientation and packing of the hydrocarbon chains are independent of surface coverage over 2 orders of magnitude in Γ. At no point in the adsorption isotherm does SFS detect any asymmetry in the adsorbed layer, excluding the possibility that hemimicelles or partial monolayers form in the first plateau of the isotherm. We have argued that there is a continuous spectrum of adsorbate behavior between the self-assembled monolayer limit and weak adsorption limit, governed by the balance of headgroup binding and hydrophobic association. While the conclusions we have presented here are specific to systems with a similar balance of interactions to CTAB on silica, the methodology is applicable to a wide range of surfactant-substrate combinations.

Acknowledgment. Funding by the European Community's Marie Curie Research Training Network "Self Organisation under Confinement (SOCON)", contract number MRTN-CT-2004-512331 is gratefully acknowledged. We thank P. A. Ash for assistance with the 2D Raman correlation analysis.

Supporting Information Available: 2-D Correlation analysis of trimethyl ammonium vibrational modes in Raman spectra; fitting parameters for SF spectra; selected sum-frequency spectra collected under the PPP and SPS polarization; enlarged SSP spectra. This material is available free of charge via the Internet at http://pubs.acs.org.

JA805169Z

(66) Noda, I.; Osaki, Y. Two-Dimensional Correlation Spectroscopy. *Applications in Vibrational and Optical Spectroscopy*; Wiley: Chichester, 2004; p 295.
(67) Morita, S. *2Dshige*, Kwansei-Gakuin University: Kwansei, 2004−2005.